The Double White Dwarf Merger Progenitors of SDSS J2211+1136 and ZTF J1901+1458

M. F. Sousa[1,2] , J. G. Coelho[1,3] , J. C. N. de Araujo[1] , S. O. Kepler[4] , and J. A. Rueda[2,5,6,7]

[1] Divisão de Astrofísica, Instituto Nacional de Pesquisas Espaciais, Avenida dos Astronautas 1758, 12227–010, São José dos Campos, SP, Brazil; manoelfelipesousa@gmail.com
[2] ICRANet-Ferrara, Dip. di Fisica e Scienze della Terra, Università degli Studi di Ferrara, Via Saragat 1, I–44122 Ferrara, Italy
[3] Núcleo de Astrofísica e Cosmologia (Cosmo-Ufes) & Departamento de Física, Universidade Federal do Espírito Santo, 29075–910, Vitória, ES, Brazil
[4] Instituto de Física, Universidade Federal do Rio Grande do Sul, 91501-970 Porto Alegre, RS, Brazil
[5] ICRANet, Piazza della Repubblica 10, I-65122 Pescara, Italy
[6] Dip. di Fisica e Scienze della Terra, Università degli Studi di Ferrara, Via Saragat 1, I–44122 Ferrara, Italy
[7] INAF, Istituto di Astrofisica e Planetologia Spaziali, Via Fosso del Cavaliere 100, I-00133 Rome, Italy

Abstract

Double white dwarf (DWD) mergers are possibly the leading formation channel of massive, rapidly rotating, high-field magnetic white dwarfs (HFMWDs). However, a direct link connecting a DWD merger to any observed HFMWD is still missing. We here show that the HFMWDs SDSS J221141.80+113604.4 (hereafter J2211+1136) and ZTF J190132.9+145808.7 (hereafter J1901+1458) might be DWD merger products. J2211+1136 is a 1.27 $M_\odot$ white dwarf (WD) with a rotation period of 70.32 s and a surface magnetic field of 15 MG. J1901+1458 is a 1.327–1.365 $M_\odot$ WD with a rotation period of 416.20 s, and a surface magnetic field in the range 600–900 MG. With the assumption of single-star evolution and the currently measured WD masses and surface temperatures, the cooling ages of J2211+1136 and J1901+1458 are, respectively, 2.61–2.85 Gyr and 10–100 Myr. We hypothesize that these WDs are DWD merger products and compute the evolution of the postmerged configuration formed by a central WD surrounded by a disk. We show that the postmerger system evolves through three phases depending on whether accretion, mass ejection (propeller), or magnetic braking dominates the torque onto the central WD. We calculate the time the WD spends in each of these phases and obtain the accretion rate and disk mass for which the WD rotational age, i.e., the total time elapsed since the merger to the instant where the WD central remnant reaches the current measured rotation period, agrees with the estimated WD cooling age. We infer the mass values of the primary and secondary WD components of the DWD merger that lead to a postmerger evolution consistent with the observations.

1. Introduction

It has long been proposed that double white dwarf (DWD) mergers can produce high-field magnetic white dwarfs (HFMWDs; see, e.g., Wickramasinghe & Ferrario 2000). There are increasing observational results pointing to this scenario (see below), but still a direct link is missing connecting a DWD merger to any observed HFMWD. Here, we aim to provide such a link.

In general, the central remnant of a DWD merger can be (i) a stable newborn white dwarf (WD), (ii) a type-Ia supernova (SN Ia), or (iii) a newborn neutron star (NS). Sub-Chandrasekhar remnants might end either as (i) or (ii) (Benz et al. 1990; Raskin et al. 2012; Zhu et al. 2013; Becerra et al. 2018, 2019; Schwab 2021a), super-Chandrasekhar remnants as (ii) or (iii) (Saio & Nomoto 1985; Schwab et al. 2016; Becerra et al. 2018, 2019; Schwab 2021a). We are here interested in those DWD mergers whose remnant is a stable, ultramassive ($\gtrsim 1\,M_\odot$ but sub-Chandrasekhar) HFMWD. Those central remnants might avoid unstable burning, leading to an SN Ia if their central density remains under some critical value of a few

$10^9\,\mathrm{g\,cm^{-3}}$ (see Becerra et al. 2018, for further details). Numerical simulations show that HFMWDs might indeed originate in DWD mergers (see, e.g., García-Berro et al. 2012; and Section 2 for further details). The general merged configuration is a central remnant that contains the mass of the (undisrupted) primary, surrounded by a hot corona with about half of the (disrupted) secondary mass, and a rapidly rotating Keplerian disk with roughly the other half of the secondary mass. Little mass ($\sim 10^{-3}\,M_\odot$) is ejected from the system (see Section 4 for further details). The hot and convective corona works as an efficient $\alpha\omega$-type dynamo that might lead to magnetic fields of $\lesssim 10^{10}$ G (García-Berro et al. 2012). For a recent discussion of the emergence of high magnetic fields in observed WDs, we refer the reader to Bagnulo & Landstreet (2022).

Therefore, theory tells us that stable WD remnants of DWD mergers can exist (see, e.g., Schwab 2021a). It remains to have observational support. Observations confirm the existence of HFMWDs with magnetic field strengths in the range 10^6–10^9 G (Külebi et al. 2009; Ferrario et al. 2015; Kepler et al. 2016), and that most of them are massive (see, e.g., Kepler et al. 2016). The latest measurements of the transverse velocities of massive WDs also suggest that a fraction of them are DWD merger products (see Cheng et al. 2020, and references therein). There is an additional observational argument supporting this conclusion. The rate of DWD mergers is

expected to be $(5–9) \times 10^{-13}$ yr$^{-1} M_\odot^{-1}$ (Maoz & Halla-koun 2017; Maoz et al. 2018). Using a Milky Way–like stellar mass $6.4 \times 10^{10} M_\odot$ and the extrapolating factor of Milky Way equivalent galaxies, 0.016 Mpc^{-3} (Kalogera et al. 2001), the above rate translates into a local cosmic merger rate of $(3.7–6.7) \times 10^5$ Gpc^{-3} yr^{-1}. This merger rate is 5–8 times larger than the population of SN Ia (see, e.g., Ruiter et al. 2009). Therefore, even if we were to explain the entire SN Ia population with the double-degenerate channel, i.e., with DWD mergers, we can safely conclude that many DWD mergers do not produce SNe Ia (see also Cheng et al. 2020).

All the above leads to a rather obvious question (but with no obvious answer), where and which are the WDs produced by (some of) those mergers? To answer this question, we here reconstruct the DWD progenitor of two recently detected HFMWDs, SDSS J221141.80+113604.4 (hereafter J2211 +1136; Kilic et al. 2021b) and ZTF J190132.9+145808.7 (hereafter J1901+1458; Caiazzo et al. 2021). J2211+1136 has a mass of $1.27 M_\odot$, rotation period of 70.32 s, surface magnetic field strength of 15 MG, effective temperature $T_{\rm eff} \approx 9020$ K, and cooling age 2.61–2.85 Gyr (Kilic et al. 2021a, 2021b). The corresponding parameters of J1901+1458 are a mass in the range of 1.327–1.365 $M_\odot$, rotation period of 416.20 s, surface magnetic field in the range 600–900 MG, effective temperature $T_{\rm eff} = 46{,}000^{+19000}_{-8000}$ K, and cooling age 10–100 Myr (Caiazzo et al. 2021). The cooling age is estimated assuming single-star evolution and the currently measured WD masses and effective temperatures.

Following numerical simulations of DWD mergers, we model the postmerger configuration as a central HFMWD remnant surrounded by a Keplerian disk (see Section 2 for details). We compute the postmerger rotational evolution of the system and infer the model parameters for which the WD rotational age, i.e., the time at which it reaches the current value of the rotation period, agrees with the estimated cooling age. We show that the postmerger configuration evolves through three phases dominated by accretion, mass ejection (propeller), and magnetic braking (see Section 3 for details). The latter phase dominates the duration of the rotational age. We derive the accretion rate, the disk mass, and the mass of the premerger DWD primary and secondary binary components for which the postmerger system agrees with observations.

We organize the article as follows. In Section 2, we summarize the properties of the merged configuration derived from numerical simulations that serve as the starting point of our calculations. Section 3 describes the theoretical treatment to compute the rotational evolution of the postmerger configuration. Section 4 explains the different types of rotational evolution. We apply in Section 5 the theoretical model to the HFMWDs J2211+1136 and J1901+1458. In Section 6, we infer the parameters of the premerger DWD progenitors for the two sources. Finally, Section 7 outlines the conclusions of this article.

2. Merger and Postmerger Properties

According to numerical simulations of DWD mergers (see, e.g., Benz et al. 1990; Guerrero et al. 2004; Lorén-Aguilar et al. 2009; Longland et al. 2012; Raskin et al. 2012; Zhu et al. 2013; Dan et al. 2014; Becerra et al. 2018), the merged configuration is the central, rigidly rotating, isothermal WD core of mass $M_{\rm core}$, surrounded by a hot envelope of mass $M_{\rm env}$ with differential rotation and a rapidly rotating Keplerian disk

of mass M_d. The mass of the disrupted secondary star distributes between the envelope and the disk. Some material of mass $M_{\rm fb}$ falls back onto the WD remnant, and only a tiny amount of mass $M_{\rm ej}$ escapes from the system. Dan et al. (2014) obtained the following fitting polynomials of the properties of the merged configurations from numerical simulations of DWD mergers for a variety of initial conditions:

$$M_{\rm core} = M_{\rm tot}(0.7786 - 0.5114\, q), \tag{1a}$$

$$M_{\rm env} = M_{\rm tot}(0.2779 - 0.464\, q + 0.7161\, q^2), \tag{1b}$$

$$M_d = M_{\rm tot}(-0.1185 + 0.9763\, q - 0.6559\, q^2), \tag{1c}$$

$$M_{\rm fb} = M_{\rm tot}(0.07064 - 0.0648\, q), \tag{1d}$$

$$M_{\rm ej} = \frac{0.0001807 M_{\rm tot}}{-0.01672 + 0.2463\, q - 0.6982\, q^2 + q^3}, \tag{1e}$$

where $M_{\rm tot} = M_1 + M_2$ is the total binary mass, with M_1 and M_2 the masses of the primary and secondary, and $q \equiv M_2/M_1 \leqslant 1$ is the binary mass ratio. The goodness of the polynomial fitting was reported in Dan et al. (2014) with R^2 statistic values of 0.97, 0.88, 0.78, and 0.8, respectively, for the first four fitting functions (1a)–(1d), which means they fit the 97%, 88%, 78%, and 80% of the corresponding variance.

We model the postmerger evolution after the short-lived phase in which the WD core incorporates the envelope. The postmerger system is thus composed of the WD remnant of mass M, radius R, surrounded by the accretion disk of mass M_d. As for the magnetic field configuration, we adopt a dipole +quadrupole model with a dipole strength B and a quadrupole strength $B_{\rm quad}$. Hence, the magnetic dipole moment is $\mu = BR^3$.

For fixed $M_{\rm tot}$, Equation (1e) shows that the unbound mass decreases for increasing q, so the lowest value is obtained for the largest possible binary mass ratio ($q = 1$), i.e., $M_{\rm ej} \approx 3.4 \times 10^{-4} M_{\rm tot}$. Given the approximate mass conservation, we estimate the mass of the final WD by

$$M = M_{\rm core} + M_{\rm env} + M_{\rm fb} + M_{\rm acc}, \tag{2}$$

where $M_{\rm acc} \leqslant M_d$ is the accreted mass. As we shall show, $M < M_{\rm tot}$ because some mass is ejected from the system during the propeller phase (see more details in Section 4). With the aid of Equations (1a)–(1e), Equation (2), and the estimate of the accreted mass, in Section 6 we estimate the parameters of the merging binary.

In the following calculations, we assume a constant value of M given by the current value of the mass of the WD, i.e., the final value given by Equation (2), neglecting the effect of the increase in mass, $M_{\rm acc}$. We also assume a constant accretion rate onto the central WD, $\dot{M}$. These assumptions have a negligible effect on the results because mass accretion and ejection consume the disk mass in a timescale much shorter than the WD lifetime, and so magnetic braking dominates the rotational evolution.

3. Postmerger Rotational Evolution

3.1. Accretion and Propeller Torque

When the magnetosphere radius, R_m, is smaller than the WD radius, R, the disk extends up to the WD surface, i.e., $r_i = R$. When $R_m > R$, the disk extends up to $r_i = R_m$. Therefore, we have

$$r_i = \max(R, R_m), \tag{3}$$

where R_m is the Alfvén radius[8] (see, e.g., Pringle & Rees 1972):

$$R_m = \left(\frac{\mu^2}{\dot{M}\sqrt{2GM}} \right)^{2/7}. \tag{4}$$

From Equation (4), we obtain that the condition $R_m > R$ is satisfied for accretion rates

$$\frac{\dot{M}}{M_\odot \, \mathrm{yr}^{-1}} < 9.74 \times 10^{-4} \frac{B_8^2 \, R_8^{5/2}}{(M/M_\odot)^{1/2}}, \tag{5}$$

where $B_8 = B/(10^8 \, \mathrm{G})$ and $R_8 = R/(10^8 \, \mathrm{cm})$.

As we shall see, the accretion rate onto the remnant WD is much lower than the above value, so the WD evolves always in the regime $R_m > R$. In this case, the magnetic field lines thread the disk at $r_i = R_m$ and the matter flows from the disk to the WD through the magnetic field lines. Whether this mass flow spins up or down the central WD depends on the value of the so-called *fastness* parameter:

$$\omega \equiv \frac{\Omega}{\Omega_K}, \tag{6}$$

where Ω_K is the Keplerian angular velocity at $r_i = R_m$:

$$\Omega_K = \sqrt{\frac{GM}{R_m^3}}. \tag{7}$$

The specific (i.e., per unit mass) angular momentum of the matter leaving the disk is $l_i = \Omega_K r_i^2 = \Omega_K R_m^2 = \sqrt{GMR_m}$, while the specific angular momentum of the corotating magnetosphere at $r = R_m$ is $l_m = \Omega R_m^2$. Therefore, the WD will change its angular momentum at a rate given by (Menou et al. 1999)

$$\dot{J}_{\mathrm{acc}} = T_{\mathrm{acc}} = (l_i - l_m)\dot{M} = \delta(1 - \omega), \tag{8}$$

where

$$\delta \equiv \dot{M} R_m^2 \, \Omega_K = \dot{M}\sqrt{GMR_m}, \tag{9}$$

$\dot{M}$ being the accretion rate, i.e., the rate at which mass flows from the disk to the WD at the inner disk radius, $r = r_i = R_m$. When $\omega < 1$, the inflowing material accretes onto the WD and transfers angular momentum to it (exerts a positive torque). When $\omega > 1$, the system enters into a so-called *propeller* regime, in which the WD centrifugal barrier expels the inflowing mass from the disk. Such mass leaves the system removing angular momentum from the central WD, i.e., it exerts a negative torque onto it. For additional discussions about the propeller mechanism, we refer the reader to, for example, Illarionov & Sunyaev (1975) and Wang (1995).

3.2. Magnetic Dipole Torque

The central remnant is also subjected to the torque by the magnetic field. Since the ratio between the stellar radius, R, and the light-cylinder radius, $R_{\mathrm{lc}} = c/\Omega$, is small, i.e., $R/R_{\mathrm{lc}} = \Omega R/c \lesssim 10^{-3}$, finite-size effects in the determination of the radiation field can be safely neglected. Therefore, we use the torque exerted by a point-like dipole+quadrupole magnetic field configuration (Pétri 2015):

$$T_{\mathrm{mag}} = T_{\mathrm{dip}} + T_{\mathrm{quad}}, \tag{10}$$

$$T_{\mathrm{dip}} = -k_{\mathrm{dip}} \, \Omega^3, \tag{11}$$

$$T_{\mathrm{quad}} = -k_{\mathrm{quad}} \, \Omega^5, \tag{12}$$

where

$$k_{\mathrm{dip}} = \frac{2}{3} \frac{B^2 R^6}{c^3} \sin^2\theta, \tag{13}$$

$$k_{\mathrm{quad}} = \frac{32}{135} \frac{B_{\mathrm{quad}}^2 R^8}{c^5} \sin^2\theta_1 (\cos^2\theta_2 + 10\sin^2\theta_2), \tag{14}$$

θ being the inclination angle of the magnetic dipole moment with respect to the WD rotation axis, and the angles θ_1 and θ_2 specifying the geometry of the quadrupole field. We can write the total magnetic torque as

$$T_{\mathrm{mag}} = -\frac{2}{3} \frac{B^2 R^6 \Omega^3}{c^3} \left(\sin^2\theta + \eta^2 \frac{16}{45} \frac{R^2 \Omega^2}{c^2} \right), \tag{15}$$

where η is a parameter that measures the quadrupole-to-dipole magnetic field strength ratio as

$$\eta = \frac{B_{\mathrm{quad}}}{B} \sqrt{\sin^2\theta_1(\cos^2\theta_2 + 10\sin^2\theta_2)}. \tag{16}$$

Having defined the torques acting on the central WD, we can write the equation of angular momentum conservation as

$$T_{\mathrm{tot}} = T_{\mathrm{acc}} + T_{\mathrm{mag}} = \dot{J} \approx I\dot{\Omega}, \tag{17}$$

whose integration gives the evolution of the WD rotational properties (e.g., angular momentum and angular velocity). The last equality neglects the change in time of the WD moment of inertia, I, as required by self-consistency with the approximation of constant mass. The above differential equation can be integrated given initial condition to the angular velocity, $\Omega_0 = \Omega(t_0 = 0)$, and setting all the model parameters, i.e., $\{M, R, I, \dot{M}, M_d, B, B_{\mathrm{quad}}, \theta, \theta_1, \theta_2, \}$. The qualitative and quantitative features of the result are not sensitive to the initial condition of the angular velocity, Ω_0. We shall explore a variety of initial rotation periods ranging from a few seconds to hundreds of seconds.

The magnetic field and the mass of the WD are set by observations (and so its radius and moment of inertia from its structure properties, e.g., mass–radius relation), so it remains to set $\dot{M}$, M_d, and θ. Without loss of generality, we shall assume an orthogonal dipole, $\theta = 90°$, and an $m = 1$ mode for the quadrupole, i.e., $(\theta_1, \theta_2) = (\pi/2, 0)$. For the disk mass, we shall set values around $M_d \approx 0.30 \, M_\odot$ according to numerical simulations (see, e.g., Dan et al. 2014, Becerra et al. 2018, and Sections 5 and 6 for details on the effect of different disk masses). Therefore, it remains only to set the value of $\dot{M}$. We shall do so by requesting that the value of Ω equals the current observed value at the evolution time consistent with estimated WD cooling age.

4. Types of Rotational Evolution

The WD might follow different types of rotational evolution depending on the model parameters and initial conditions. In the most general case, the system evolves through three stages until it reaches the current rotation period: a *phase I* of accretion (the WD spins up) or ejection of matter (the WD spins down) by propeller, a *phase II* in which accretion and matter ejection episodes balance each other so the WD spin
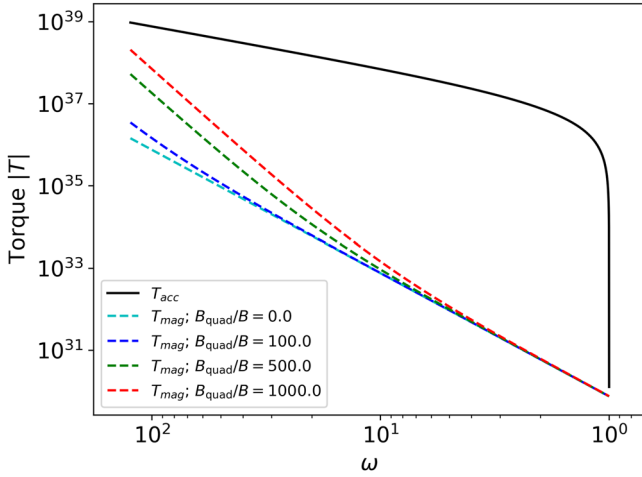
---

[8] This magnetosphere radius assumes spherical accretion and a pure dipole magnetic field configuration.

Figure 1. $|T_{\rm acc}|$ and $|T_{\rm mag}|$ as a function of $\omega > 1$ where we considered a WD with $B = 100$ MG, $\dot{M} = 10^{-7} M_\odot$ yr^{-1}, and a quadrupole-to-dipole magnetic field strength ratio $B_{\rm quad}/B$. The ratio $B_{\rm quad}/B = 0.0$ corresponds to the case of a pure dipole magnetic field.
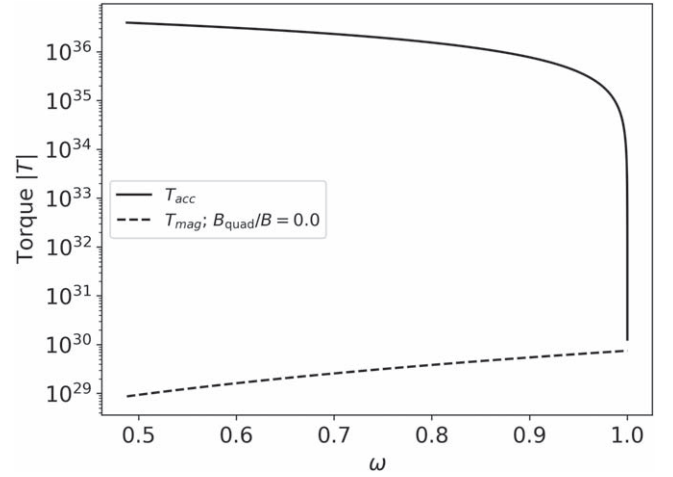

Figure 2. $|T_{\rm acc}|$ and $|T_{\rm mag}|$ as a function of $\omega < 1$ where we considered a WD with $B = 100$ MG, $\dot{M} = 10^{-7} M_\odot$ yr^{-1}, and a quadrupole-to-dipole magnetic field strength ratio $B_{\rm quad}/B = 0.0$, since the effect of the quadrupole magnetic field is very small when we take into account the values of $\omega < 1$ presented here (See Equation (15)).

remains at an equilibrium value, and a *phase III* which the system enters once the disk mass ends, so the WD spins down because of magnetic braking.

Because DWD mergers always form a debris disk around the newborn central remnant (see, e.g., Lorén-Aguilar et al. 2009; Dan et al. 2014), we rule out an evolution with only phase III, i.e., without either accretion or matter ejection and only evolving due to magnetic braking. Therefore, the postmerger WD necessarily starts its evolution either at the phase I or II.

We now focus on the most general case, i.e., when the system evolves through the above three stages until it reaches the current rotation period. The division of the evolution into three phases depends on the value of the fastness parameter, that is, $\omega > 1$, $\omega \approx 1$, and $\omega < 1$. Depending on the initial angular velocity, Ω_0, the initial value of the fastness parameter can either be $\omega_0 > 1$ ($\Omega_0 > \Omega_K$) or $\omega_0 < 1$ ($\Omega_0 < \Omega_K$). The torque, $T_{\rm acc}$, is either negative when the propeller mechanism is active ($\omega > 1$) or positive when the accretion process is active ($\omega < 1$). On the other hand, the magnetic torque, $T_{\rm mag}$, always removes angular momentum. When there is mass flowing from the inner radius of the disk, the propeller or the accretion dominates the changes in the rotational period given that $T_{\rm acc}$ dominates over $T_{\rm mag}$. Figure 1 shows $T_{\rm acc}$ and $T_{\rm mag}$ as a function of $\omega > 1$ up to the value of $\omega \approx 1$, for fiducial values of the dipole magnetic field and the accretion rate, respectively, $B = 100$ MG, and $\dot{M} = 10^{-7} M_\odot$ yr^{-1}. We consider $T_{\rm mag}$ with different values of $B_{\rm quad}/B$ in order to assess the effect of $B_{\rm quad}$ on the spin evolution. Figure 2 is analogous to Figure 1 but for $\omega < 1$. Here, we only consider the pure magnetic dipole case, $B_{\rm quad}/B = 0$, because for low values of the angular velocity the torque by the quadrupole magnetic field is very small compared to that produced by the magnetic dipole (see Equation (15)). These figures show that $|T_{\rm acc}| \gg |T_{\rm dip}|$ for the entire present phase, with the only exception being when $\omega \approx 1$, where they become comparable as $T_{\rm acc}$ drops significantly.

It is worth mentioning that for $B_{\rm quad}/B = 1000$, the intensity of $T_{\rm mag}$ approaches the intensity of $T_{\rm acc}$ for values of the angular velocity around a few seconds. However, when the angular velocity decreases, $T_{\rm mag}$ drops rapidly while $T_{\rm acc}$ remains high for nearly the entire phase of $\omega > 1$. Thus, $T_{\rm acc}$

still dominates the torque and $T_{\rm mag}$ (even with $B_{\rm quad}/B = 1000$) contributes very little to this first evolution stage.

Taking the above into account in this first regime, we can approximate with sufficient accuracy the total torque by $T_{\rm tot} \approx T_{\rm acc}$. Within this approximation, Equation (17) has the analytic solution

$$\omega = 1 + (\omega_0 - 1)e^{-t/\tau_{\rm acc}}, \tag{18}$$

where $\omega_0 = \Omega_0/\Omega_K$ is initial fastness parameter and $\tau_{\rm acc}$ is the timescale (e-folding time) of the propeller/accretion phase:

$$\tau_{\rm acc} = \frac{I\,\Omega_K}{\delta} = \frac{I}{\dot{M}R_m^2} = 50.27 \frac{I_{49}}{\dot{M}_{-7}R_{m,9}^2}\ {\rm kyr}, \tag{19}$$

where I_{49} is the moment of inertia in units of 10^{49} g cm^2, $\dot{M}_{-7}$ is the accretion rate in units of $10^{-7} M_\odot$ yr^{-1} and $R_{m,9}$ is the Alfvén radius in units of 10^9 cm.

When $\omega \approx 1$, the WD enters phase II of evolution, characterized by $T_{\rm acc} \approx T_{\rm mag}$. When this occurs, $T_{\rm mag}$ decelerates the star to an angular velocity slightly smaller than Ω_K, so to a fastness parameter $\omega \lesssim 1$. Then, $T_{\rm acc}$ turns positive and the WD accretes matter, spinning it up. This happens until the WD returns once more to the regime of $\omega \gtrsim 1$. Upon reaching this regime, due to the torques $T_{\rm acc}$ and $T_{\rm mag}$, the WD rotation decelerates once more until $\omega \lesssim 1$. The accretion acts, and the propeller process ceases again. In summary, in this stage the WD goes through successive spin-up and spin-down stages in which the fastness parameter oscillates around unity, so the angular velocity oscillates around an *equilibrium* value, $\Omega \approx \Omega_{\rm eq} = \Omega_K$. Therefore, we can assume that in this phase Ω remains constant at

$$\Omega_{\rm eq} = \Omega_K = \left[\frac{\sqrt{2}\,(GM)^{5/3}\,\dot{M}}{B^2\,R^6} \right]^{3/7}$$

$$= 0.225 \left[\frac{(M/M_\odot)^{5/3}\,\dot{M}_{-7}}{B_8^2\,R_8^6} \right]^{3/7}\ {\rm rad\ s}^{-1}. \tag{20}$$

This phase lasts until the disk can feed the accretion and propeller. Thus, the duration timescale of this phase is of the

order $\tau_{disk} \approx M_d/\dot{M} \sim 10^6$ yr, that is, the time required to consume the disk mass.

After the disk is exhausted, the system evolves to the regime $\omega < 1$. Without mass flowing from the disk, only the magnetic dipole exerts torque. Equation (15) and Figure 1 show that the effect of the quadrupole magnetic field on the magnetic torque is negligible in the range of angular velocities of the regime $\omega \lesssim 1$. In this case, the torque due to dipole radiation dominates and we can accurately approximate the total torque by $T_{tot} = T_{mag} \approx T_{dip}$. Thus, we can solve Equation (17) analytically:

$$\omega = \left(1 + \frac{\Delta t}{\tau_{dip}}\right)^{-1/2}, \qquad (21)$$

where $\delta t = t - t_i$, with t_i being the initial time of the pure magnetic dipole torque phase, and here we have assumed that this phase starts with an initial value of the fastness parameter equal to unity, i.e., $\omega(t = t_i) = 1$. The characteristic spin-down timescale, τ_{dip}, is given by

$$\tau_{dip} = \frac{I}{2 \, k_{dip} \, \Omega_K^2} = \frac{c^3 I R_m^3}{2GMB^2R^3(1 + \sin^2\theta)}$$

$$= 3.22 \frac{I_{49}R_{m,9}^3}{(M/M_\odot)B_8^2R_8^3(1 + \sin^2\theta)} \text{ Gyr}, \qquad (22)$$

which is much longer than the timescale of the previous phases. The above implies that we can approximate the total postmerger age of the WD to the time it spends in this final phase.

We can invert Equation (21) and find the elapsed time, Δt_{obs}, for the WD to reach an observed angular velocity, Ω_{obs}, i.e.,

$$\Delta t_{obs} = \tau_{dip}\left[\left(\frac{\Omega_K}{\Omega_{obs}}\right)^2 - 1\right]. \qquad (23)$$

Since τ_{dip} depends on Ω_K and the latter depends on R_m, and so on $\dot{M}$, we can use Equation (23) to express $\dot{M}$ in terms of Ω_{obs} and Δt_{obs}:

$$\dot{M} = \frac{B^2R^6\,\Omega_{obs}^{7/3}}{\sqrt{2}\,(GM)^{5/3}}\left(1 - \frac{2\,k_{dip}\,\Omega_{obs}^2}{I}\Delta t_{obs}\right)^{-7/6}. \qquad (24)$$

Therefore, Equation (24) allows one to obtain, from observational parameters such as mass, angular velocity, magnetic field, and the estimated age of the WD (e.g., the cooling age), the accretion rate for which the rotational evolution agrees with observations.

5. Analysis of Specific Sources

Having described all the generalities of the postmerger evolution, we turn to describe the rotational evolution of two observed HFMWDs, namely, J2211+1136 and J1901+1458. We infer the time the WD spends in each phase, and calculate the accretion rate that leads to the rotational evolution to agree with the estimated WD cooling age. This assumption agrees with the fact that the cooling tracks of these sources are estimated considering the current mass of the WD, so the cooling age is the evolution time of the postmerger central remnant after the envelope has been fully incorporated into the isothermal core and the WD composition has settled down (see, e.g., Schwab 2021b, for more details). The above is also
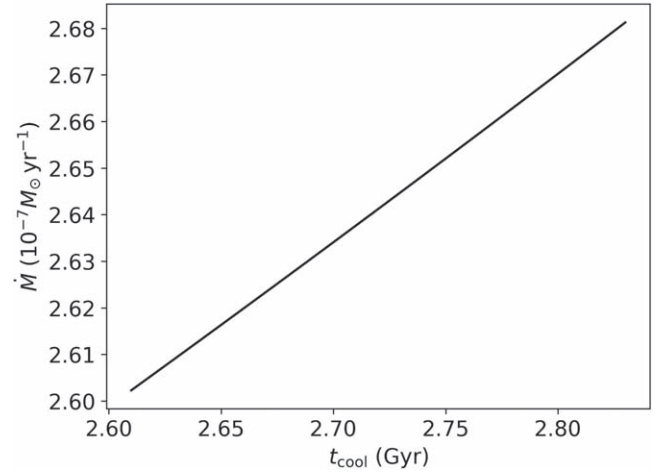

Figure 3. Accretion rate as a function of cooling age, calculated from Equation (24), for J2211+1136. The WD parameters are $M = 1.27\, M_\odot$, $R = 3.21 \times 10^8$ cm, and $P_{obs} = 70.3$ s. The dipole magnetic field is $B = 15$ MG and $\theta = 90°$.

supported by the fact that the initial phase of fusion containing the envelope is short lived ($\sim 10^4$–10^5 yr; see, e.g., García-Berro et al. 2012; Schwab 2021a) compared to the estimated age of the WD and, as we show in this article, also the duration of the accreting phase is negligible.

We do not take into account any delay due to crystallization, phase separation due to sinking or dilution of heavier elements, or nuclear energy that can possibly occur as proposed, for example, by Cheng (2020) and Blouin & Daligault (2021).

5.1. Rotational Evolution of J2211+1136

J2211+1136 is a recently observed isolated WD with a rotation period $P_{obs} = 70.32$ s (Kilic et al. 2021b). It has a mass $M = 1.27\, M_\odot$, a stellar radius $R = 3210$ km,[9] and a surface (dipole) magnetic field $B = 15$ MG. The cooling age is in the range $t_{cool} = 2.61$–2.85 Gyr depending on the WD interior composition (Kilic et al. 2021a, 2021b).

First, to explore the evolutionary path of the WD rotation, we need to know the accretion rate values for which the rotational evolution time agrees with the cooling age. For this task, we use Equation (24), assuming $\Delta t_{obs} = t_{cool}$. Figure 3 shows that this condition implies that $\dot{M}$ must be in the range $\approx (2.60$–$2.68) \times 10^{-7}\, M_\odot$ yr^{-1}. For an aligned rotator ($\theta = 0$), the corresponding accretion rate range is $(2.21$–$2.24) \times 10^{-7}$ $M_\odot$ yr^{-1}.

To analyze in detail the phases of spin evolution, we consider a value of $\dot{M}$ within the above range, e.g., $\dot{M} = 2.62 \times 10^{-7} M_\odot$ yr^{-1}. Furthermore, we consider six values for the initial rotation period to verify that the solution is not sensitive to this initial condition. For this task, we choose three values below and three values above the equilibrium period, $P_{eq} = 2\pi/\Omega_{eq} \approx 61.5$ s, i.e., $P_0 = (3.14, 21.5, 41.5, 81.5, 101.5, 119.8)$ s. Figure 4 shows the evolution of the WD rotation period for these initial conditions. We observe that, irrespective of P_0, the WD accelerates or decelerates toward P_{eq} on a comparable timescale. Therefore, the duration of the rotational evolution in phase I is not sensitive to the specific value of P_0.

---

[9] We estimate the radius from the measured mass and surface gravity, $\log(g) = 9.214$ (Kilic et al. 2021b), i.e., $R = \sqrt{GM/g}$.
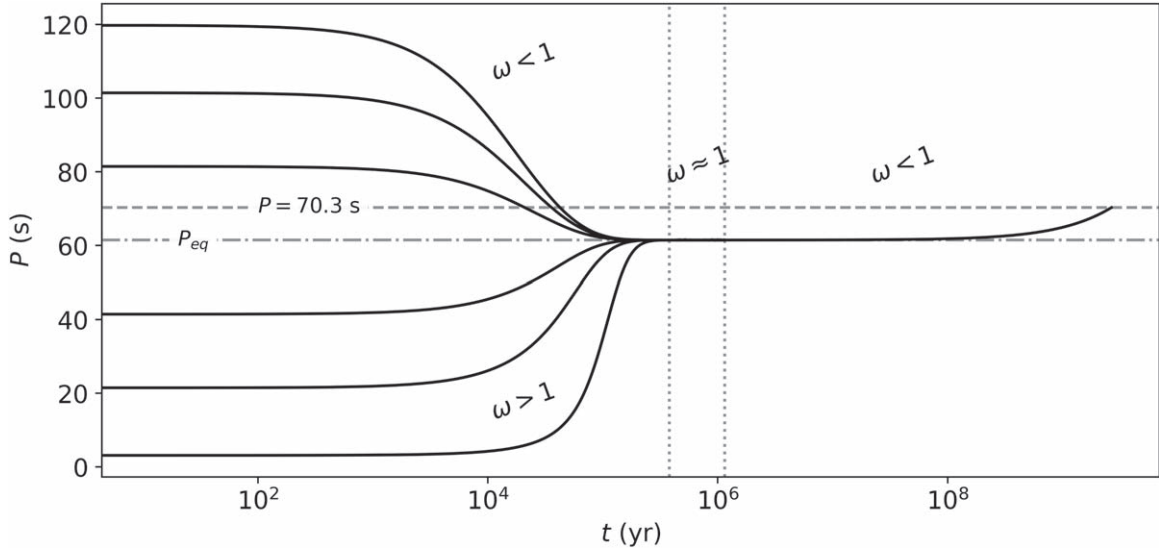
Figure 4. Evolution of the rotation period of the J2211+1136 for an accretion rate of $\dot{M} = 2.62 \times 10^{-7} M_\odot \, \mathrm{yr}^{-1}$ and for different values of initial rotational periods, $P_0 = (3.14, 21.5, 41.5, 81.5, 101.5, 119.8)$ s. The dotted lines divide the evolution into three stages according to the value of ω. In the first stage, the WD can start with $\omega > 1$ or $\omega < 1$ depending whether the initial period is below or above the equilibrium period, $P_{eq} = 61.15$ s (Equation (20)), respectively. For both values, the involved torques are magnetic torque, T_{mag}, and accretion torque, T_{acc}. However, T_{acc} is the dominant torque in this phase. For $\omega \approx 1$, $T_{mag} \approx T_{acc}$ and the system goes through the P_{eq}. For $\omega < 1$, the involved torque is T_{mag}. T_{acc} no longer acts on the star, as in the third stage the disk has already been exhausted. The upper dashed line indicates the current rotation period of the WD.

Because of the above result, we examine in detail the evolution curve for a single case, e.g., $P_0 = 3.14$ s. For the parameters of this WD, and a $M_d = 0.30 \, M_\odot$, which lies within the range of consistent values obtained for the disk mass and numerical simulations (see Section 6 for more details), the evolution of the rotation period of J2211+1136 crosses the three stages until it reaches the current value of the rotation period. First, it passes through the regime of $\omega > 1$, such that the torques T_{acc} and T_{dip} spin-down the WD to a period of 61.5 s in $\Delta t_1 \approx 0.37$ Myr. This time is marked by the first dotted line in Figure 4. The amount of disk mass ejected by the propeller effect during this time is $M_{loss,1} = \dot{M} \Delta t_1 \approx 0.096 \, M_\odot$.

From this period value, the parameter $\omega \approx 1$ and the system enters the equilibrium period regime, where the WD rotation period is oscillating around P_{eq} (see Equation (20)). The system remains at this stage until the disk mass ends. The phase lasts $\Delta t_2 \approx 0.78$ Myr. Therewith, adding the duration of the first and second stages, we have up to this point an evolution time of $\Delta t_1 + \Delta t_2 \approx 1.15$ Myr. This time is marked by the second dotted line in Figure 4. In this phase II, the disk mass loss is divided in equal parts in accretion and ejection, so $M_{acc,2} = M_{loss,2} = (1/2)\dot{M}\Delta t_2 \approx 0.102 \, M_\odot$. Therefore, by the end of phase II, the total disk mass has indeed been consumed, i.e., $0.096 \, M_\odot + 0.204 \, M_\odot = M_d$. The disk mass has been distributed in a total ejected mass $M_{loss} = M_{loss,1} + M_{loss,2} \approx 0.2 \, M_\odot$ and a total accreted mass $M_{acc} = M_{acc,2} \approx 0.1 \, M_\odot$.

After this point, the system enters the regime of $\omega < 1$, where the only active torque is T_{mag}. Thus, T_{mag} spins the WD down from a period of 61.5 s to the observed period $P_{obs} = 70.3$ s, reached at a time of 2.66 Gyr (see Figure 4). Phase III is by far the longest, so the WD spends most of its evolution in this regime.

In addition to the agreement of the rotational and cooling ages, the full proof of the present scenario would arise from the further agreement of the model spin-down rate with corresponding observational measurement (see, e.g., the case of 4U

0142+61 in Rueda et al. 2013). For the magnetic dipole braking mechanism (see Equation (15)), the spin-down rate is given by

$$\dot{P} = \frac{8\pi^2}{3c^3} \frac{R^6 B^2}{I P_{obs}} \sin^2 \theta. \qquad (25)$$

For J2211+1136, adopting $R = 3210$ km, $I = (2/5)MR^2 = 1.04 \times 10^{50}$ g cm^2, and $B = 15$ MG, we obtain $\dot{P} \approx 3.3 \times 10^{-17} \sin^2 \theta$ s s^{-1} (see also Williams et al. 2022). This spin-down rate is too low to be detected, e.g., two orders of magnitude lower than the one of the pulsating WD G 117-B15A, $\dot{P} \approx 5.12 \times 10^{-15}$ s s^{-1} (Kepler et al. 2021).

5.2. Rotational Evolution of J1901+1458

J1901+1458 has a period of rotation $P_{obs} = 416.2$ s, a mass $M = 1.327$–$1.365 \, M_\odot$, a stellar radius $R = 2140^{+160}_{-230}$ km, and a surface (dipole) magnetic field in the range $B = 600$–900 MG. The cooling age is $t_{cool} = 10$–100 Myr (Caiazzo et al. 2021). For simplicity, we consider $M = 1.35 \, M_\odot$ with $R = 2140$ km in the analysis of this source. Furthermore, we follow the analogous procedure described above for J2211+1136. We analyze the evolution of the WD rotation period for different values of the initial rotation period, a disk mass of $M_d = 0.34 \, M_\odot$ consistent with the range of values obtained in Section 6, and a value of $\dot{M}$ consistent with Equation (24). We use a dipole magnetic field strength of $B = 800$ MG, inferred in Caiazzo et al. (2021) from the analysis of the position of the Hα, Hβ, and Hγ spectral lines.

Using Equation (24), we obtain the accretion rate as a function of t_{cool}. Considering $\theta = 90°$, we obtain $\dot{M} \approx (6.92$ –$8.05) \times 10^{-7} M_\odot \, \mathrm{yr}^{-1}$ (See Figure 5). For an aligned rotator, $\dot{M} \approx (6.87$–$7.39) \times 10^{-7} \, M_\odot \, \mathrm{yr}^{-1}$. Figure 6 shows the rotation-period evolution for $\dot{M} = 8.0 \times 10^{-7} M_\odot \, \mathrm{yr}^{-1}$, and initial values of the rotation period $P_0 = (3.14, 108.7, 258.7, 558.7, 708.7, 814.2)$ s. The curves approach the equilibrium period, P_{eq}, in a timescale of the same order of magnitude.
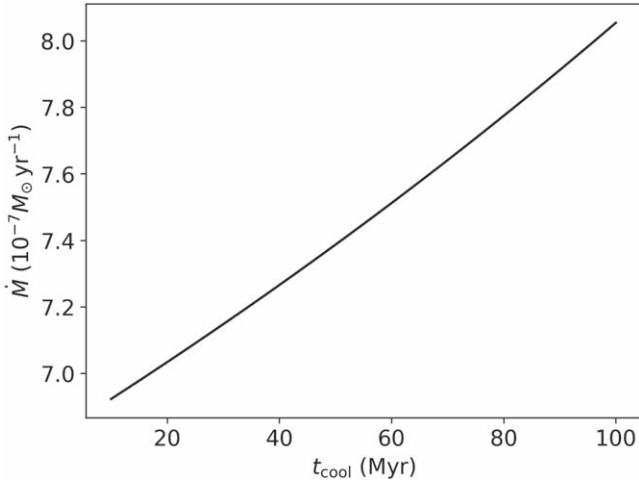
Figure 5. Accretion rate as a function of cooling age calculated from Equation (24) for J1901+1458. The WD parameters are $M = 1.35\ M_\odot$, $R = 2.14 \times 10^8$ cm, $P_0 = 3.14$ s, and $P_{obs} = 416.2$ s. The magnetic field strength is $B = 800$ MG and $\theta = 90°$.

Thus, also for this source, we see that the final evolution time is not affected by the choice of the initial period.

Without loss of generality, we now describe the phases of the spin evolution in the case $P_0 = 3.14$ s. The system first evolves through the propeller regime $\omega > 1$, in which the WD spins down to a period of 388.6 s in $\Delta t_1 \approx 5.98$ kyr (marked by the first dotted line in Figure 6). During this time, the amount of the disk mass ejected was $M_{loss,1} = \dot{M}\Delta t_1 \approx 4.8 \times 10^{-3}M_\odot$.

After the rotation period reaches $\omega \approx 1$, the second stage starts. Thus, J1901+1458 evolves through spin-down and spin-up stages around the equilibrium period value, until the disk mass ends. We estimate that this phase lasts $\Delta t_2 \approx 0.42$ Myr. Up to this point, the postmerger evolution time adding the two stages is $\Delta t_1 + \Delta t_2 \approx 0.425$ Myr, which is marked by the second dotted line in Figure 6. In this phase II, we have $M_{acc,2} = M_{loss,2} = (1/2)\dot{M}\Delta t_2 \approx 0.168\ M_\odot$. Thus, in this source, nearly the entire disk mass is consumed in phase II, so we have a total ejected mass $M_{loss} = M_{loss,1} + M_{loss,2} \approx 0.17\ M_\odot$ and a total accreted mass $M_{acc} = M_{acc,2} \approx 0.17\ M_\odot$.

In the subsequent evolution, the only torque acting on the WD is T_{dip}, so the WD enters the phase characterized by $\omega < 1$. The WD spins down from a period of 388.6 s to the observed period $P_{obs} = 416.2$ s. This occurs in ≈ 96.2 Myr. Figure 6 shows this last stage for the spin evolution.

The spin-down rate in the current phase for J1901+1458 can be estimated from Equation (25). Adopting $R = 2140$ km, $I = (2/5)MR^2 = 5.0 \times 10^{49}$ g cm^2, and $B = 800$ MG, we obtain $\dot{P} \approx 2.9 \times 10^{-15}\sin^2\theta$ s s^{-1}, which is consistent with the upper limit value of $\dot{P} < 10^{-11}$ s s^{-1} presented in Caiazzo et al. (2021). In this case, the resulting spin-down rate is similar to the spin-down rate of G 117-B15A. Therefore, although experimentally challenging, timing analyses, as in the one done by Kepler et al. (2021) for G 117-B15A, could lead in the future to the final proof of the DWD merger scenario for J1901+1458 presented in this work.

6. The DWD Merger Progenitors

We now turn to estimate the masses of the components (M_1 and M_2) of the DWD progenitor of the above two systems. For this task, we have to estimate the binary total mass, M_{tot}, and mass ratio, q, so that

$$M_1 = \frac{1}{1+q}M_{tot}, \qquad M_2 = \frac{q}{1+q}M_{tot}. \qquad (26)$$

First, we use the fact that DWDs eject a tiny amount of mass during merger (Lorén-Aguilar et al. 2009; Dan et al. 2014), which allows us to assume baryon mass conservation with an error of at most one part in a thousand. Then, for a given disk mass, M_d, and accretion rate, $\dot{M}$, we have here obtained in the postmerger evolution the total accreted mass by the central WD remnant, M_{acc}, and the total mass loss due to action of the propeller, M_{loss}. Clearly, $M_d = M_{acc} + M_{loss}$. Therefore, we can write the total binary mass as

$$M_{tot} = M + M_{loss} + M_{ej} \approx M + M_{loss}, \qquad (27)$$

where we recall that M is the current measured mass of the WD, and M_{loss} can be written as

$$M_{loss} = \frac{M_d \pm M_{cons}}{2}, \qquad (28)$$

where the $\pm$ sign is used when phase I starts with propeller ($\omega_0 > 1$) or accretion ($\omega_0 < 1$). The quantity M_{cons} is the disk mass consumed in phase I. We now can find a equation for M_d as a function of the mass ratio, q. To do this, we substitute Equation (27) into Equation (1c) and solve it for M_d, which leads to

$$M_d = \frac{Q}{2-Q}(2M \pm M_{cons}), \qquad (29)$$

where $Q = -0.1185 + 0.9763q - 0.6559q^2$. Furthermore, we can use Equation (29) together with Equation (28) to express M_{loss} in terms of q:

$$M_{loss} = \frac{Q}{2-Q}\left(M \pm \frac{M_{cons}}{Q}\right). \qquad (30)$$

Therefore, with the equations obtained above, we can calculate M_{tot} and the masses of the components of the DWD progenitor with the following general procedure. Having chosen the initial rotation period and the accretion rate, we calculate the disk mass consumed in phase I, M_{cons}. Thus, the disk mass function $M_d = M_d(M_{cons}, q)$, given by Equation (29), and the mass loss function $M_{loss} = M_{loss}(M_{cons}, q)$, given by Equation (30), become a function of q. These functions are concave-down parabolas with maximums at q^*, so the disk mass and mass loss increase with q up to the maximum value $M_d^{max} = M_d(q^*)$ and $M_{loss}^{max} = M_{loss}(q^*)$, to then decrease up to the values $M_d(q=1)$ and $M_{loss}(q=1)$, respectively. Therefore, if $M_d \leqslant M_d(q=1)$ or $M_{loss} \leqslant M_{loss}(q=1)$, there is a unique solution for q. If $M_d > M_d(q=1)$ or $M_{loss} > M_{loss}(q=1)$, there are two solutions for q.

We shall seek for solutions with a disk mass that satisfies $M_d \gtrsim M_d^{min}$, where $M_d^{min} = 0.1\ M_\odot$ is approximately the minimum disk mass obtained in the numerical simulations of Dan et al. (2014), taking into account that $M \approx 1.3\ M_\odot$ in the two analyzed systems.

We recall that in view of the nonzero disk mass left by DWD mergers, we have already discarded solutions in which the system evolves only through phase III, i.e., only under the action of the magnetic dipole torque. Therefore, we are left with three possible cases: (i) evolution with phases I+III, (ii)
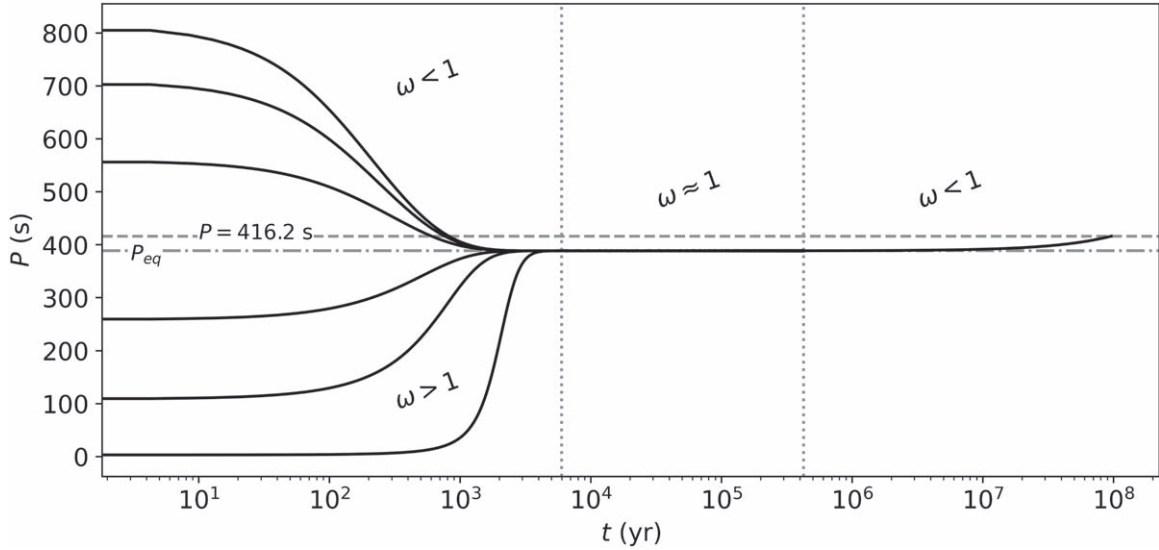
Figure 6. Evolution of spin period of the J1901+1458 for $\dot{M} = 8.0 \times 10^{-7} M_\odot$ yr^{-1} (with $B = 800$ MG) and for different values of initial rotational periods, $P_0 = (3.14, 108.7, 258.7, 558.7, 708.7, 814.2)$ s. The dotted lines divide the evolution into three stages according to the value of ω. In the first stage, the WD can start with $\omega > 1$ or $\omega < 1$ depending whether the initial period is below or above the equilibrium period, $P_{eq} = 388.6$ s (Equation (20)), respectively. For both values, the involved torques are dipole radiation torque, T_{mag}, and accretion torque, T_{acc}, in the propeller phase. However, T_{acc} is the dominant torque in this phase. For $\omega \approx 1$, $T_{mag} \approx T_{acc}$ and the system goes through the equilibrium period, P_{eq}. For $\omega < 1$, the involved torque is T_{dip}. T_{acc} no longer acts on the star, as in the third stage the disk has already been exhausted. The upper dashed line indicates the current rotation period of the WD.

with phases II+III, and, the most general case, (iii) with phases I+II+III. We now analyze each case.

6.1. Case (i): Evolution with Phases I+III

In this case, the system does not evolve through phase II, so the entire disk mass is consumed in phase I, i.e., $M_{cons} = M_d$. From Equation (28), we have that when phase I is a propeller ($\omega_0 > 1$), $M_{loss} = M_d$, while if it is an accretor ($\omega_0 < 1$), $M_{loss} = 0$. It can be shown that under these conditions, to satisfy the boundary condition of approximate equality of the rotational and the cooling age, either the disk mass must be $M_d \ll M_d^{min} = 0.1\,M_\odot$ or the accretion rate must have very large values $\gtrsim 10^{-5}\,M_\odot$ yr^{-1}. Therefore, we do not consider this case as astrophysically viable.

6.2. Case (ii): Evolution with Phases II+III

In this case, the initial angular velocity satisfies $\Omega_0 = \Omega_{eq}$, so there is no phase I and the disk mass is divided in equal parts into accretion and propeller. We have $M_{cons} = 0$, so Equation (28) leads to $M_{loss} = M_d/2$.

6.3. Case (iii): Evolution with Phases I+II+III

In this general case, the system evolves through the three phases as described in Section 4. The angular velocity at the beginning of phase III, say Ω_{dip}, is approximately given by the equilibrium value, i.e., $\Omega_{dip} \approx \Omega_{eq}$. With this constraint, we can estimate M_{cons} by

$$M_{cons} \approx I\left(\frac{\Omega_{eq}^2}{GM}\right)^{2/3} \ln\left(\frac{\Omega_0 - \Omega_{eq}}{\Omega_{dip} - \Omega_{eq}}\right), \tag{31}$$

which is obtained from Equation (18), solving it for t, making $t = \Delta t_1 = M_{cons}/\dot{M}$ and $\Omega = \Omega_{dip}$. Therefore, M_{cons} lies in the range $0 < M_{cons} < M_d$.
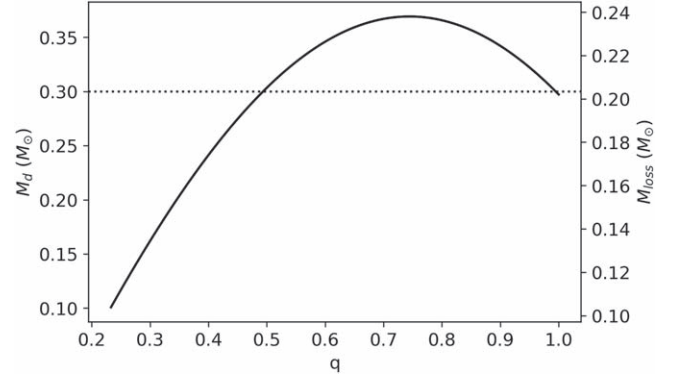

Figure 7. Disk mass, M_d, and mass loss, M_{loss}, as a function of the binary mass ratio, q. The solid curve represents the solutions for J2211+1136 ($M = 1.27\,M_\odot$, $P_0 = 3.14$ s, $\dot{M} = 2.62 \times 10^{-7} M_\odot$ yr^{-1}), while the dashed horizontal line shows the corresponding value used in the simulation.

6.4. Specific Examples

To exemplify the approach above, we consider the cases of J2211+1136 and J1901+1458 in Section 5, i.e., in the general evolution (iii) in which the system evolves through phases I+II+III. Figure 7 shows the functions $M_d(M_{cons}, q)$ and $M_{loss}(M_{cons}, q)$ for J2211+1136, given $M_{cons} \approx 0.1\,M_\odot$ ($P_0 = 3.14$ s and $\dot{M} = 2.62 \times 10^{-7} M_\odot$ yr^{-1}). Figure 8 is analogous to Figure 7 but for J1901+1458, with $M_{cons} \approx 4.8 \times 10^{-3} M_\odot$ ($P_0 = 3.14$ s and $\dot{M} = 8.0 \times 10^{-7} M_\odot$ yr^{-1}). Thus, for J2211+1136 and J1901+1458, we obtain $M_d^{max} \approx 0.36\,M_\odot$, $M_d(q = 1) \approx 0.297\,M_\odot$, and $M_d^{max} \approx 0.37\,M_\odot$, $M_d(q = 1) \approx 0.304\,M_\odot$, respectively. From the M_d^{min} and M_d^{max} values obtained above, we note that our choice for the disk mass of J2211+1136, $M_d = 0.30\,M_\odot$, and of J1901+1458, $M_d = 0.34\,M_\odot$, are within the range of physically plausible values. The horizontal dashed lines in Figures 7 and 8 represent these values and their intersection with the curve of the source gives the mass ratio q to these cases.
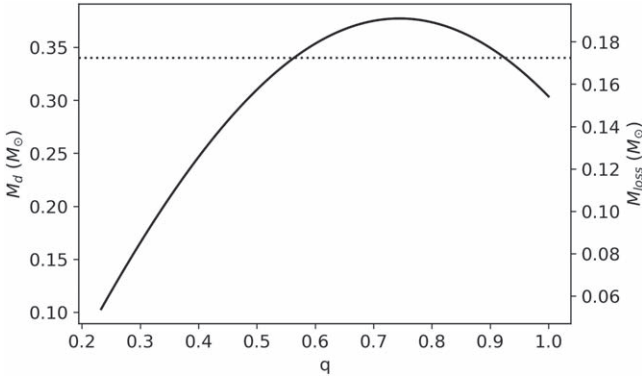
Figure 8. Disk mass, M_d, and mass loss, M_{loss}, as a function of the binary mass ratio, q. The solid curve represents the solutions for J1901+1458 ($M = 1.35\,M_\odot$, $P_0 = 3.14$ s, $\dot{M} = 8.0 \times 10^{-7} M_\odot$ yr^{-1}), while the dashed horizontal line shows the corresponding value used in the simulation.

Moreover, Figures 7 and 8 show that, given a value of q, we can estimate the M_d and M_{loss}, so we can calculate M_{tot} from Equation (27). With these values, we can obtain the primary and secondary mass via Equation (26). In Figure 9, we show the M_1–M_2 plane of possible solutions of the DWD progenitor. Each pair (M_2, M_1) in this figure corresponds to a value of q and, consequently, to a value of M_d. Therefore, we can infer the values M_1 and M_2 for the simulated cases in Section 5 taking into account the assumed value of M_d.

Therefore, since for the two systems we have chosen a disk mass value $M_d > M_d(q = 1)$, there are two possible values of mass ratio, q_a and q_b (see Figures 7 and 8). For J2211+1136, we obtain $q_a = 0.495$ and $q_b = 0.993$, while for J1901+1458, $q_a = 0.565$ and $q_b = 0.924$. For J2211+1136, the mass ratio q_a gives $M_1 = 0.983\,M_\odot$, $M_2 = 0.487\,M_\odot$, while the solution q_b gives $M_1 = 0.737\,M_\odot$, $M_2 = 0.732\,M_\odot$. For J1901+1458, the mass ratio q_a gives $M_1 = 0.971\,M_\odot$, $M_2 = 0.549\,M_\odot$, and q_b gives $M_1 = 0.790\,M_\odot$, $M_2 = 0.729\,M_\odot$. Table 1 summarizes the results of the above analysis. In particular, it lists the parameters of the premerger DWD and the parameters of the postmerger system for the disk mass and accretion rate in the simulations of Section 5.

Interestingly, the inferred parameters of the DWD progenitor of J1901+1458 and J2211+1136 (see Table 1) are consistent with the parameters of known systems, e.g., NLTT 12758, a $0.83 + 0.69\,M_\odot$ DWD (Kawka et al. 2017). This result further supports the link that we have here provided between DWD mergers and the formation of HFMWDs.

7. Discussion and Conclusions

In this article, we have investigated the possibility that the HFMWDs J2211+1136, and J1901+1458 are DWD merger products. Based on numerical simulations of DWD mergers, we have modeled the postmerger system as a central WD surrounded by a disk from which there is a mass inflow toward the WD remnant. We have calculated the postmerger rotational evolution of the WD and inferred the system parameters for which the rotational age agrees with the WD cooling age.

We have shown that the postmerger configuration evolves through three different phases depending on whether accretion, mass ejection (propeller), or magnetic braking dominate the torque on the WD. We have shown that the WD spends most of its lifetime in the third phase, in which only magnetic braking torques the WD (see Figures 4 and 6). We have used the
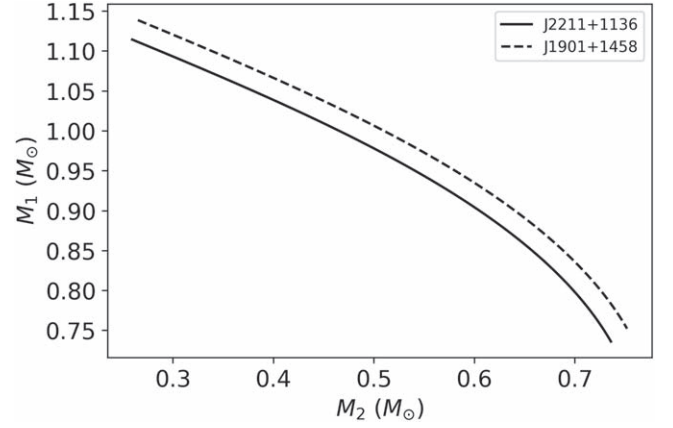

Figure 9. Predicted range of the primary and secondary mass. The solid curve represents the solutions for J2211+1136 (postmerger WD mass of $M = 1.27\,M_\odot$, $P_0 = 3.14$ s, and $\dot{M} = 2.62 \times 10^{-7} M_\odot$ yr^{-1}) and the dashed curve for J1901+1458 (postmerger WD mass of $M = 1.35\,M_\odot$, $P_0 = 3.14$ s, and $\dot{M} = 8.0 \times 10^{-7} M_\odot$ yr^{-1}).

Table 1
Parameters of the Premerger (DWD) and Postmerger (Central Remnant WD +Disk) Systems Leading to the Current Observed Parameters of J2211+1136 and J1901+1458

Parameter	J2211+1136	J1901+1458
Premerger system		
q_a, q_b	0.49, 0.99	0.56, 0.92
M_{tot} ($M_\odot$)	1.47	1.52
M_1 ($M_\odot$)	0.98, 0.74	0.97, 0.79
M_2 ($M_\odot$)	0.49, 0.73	0.55, 0.73
M_{ej} ($10^{-3}\,M_\odot$)	4.96, 0.51	3.61, 0.68
Postmerger system		
M ($M_\odot$)	1.27[a],[b]	1.35[c]
R (km)	3210	2140 [c]
P (s)	70.32[a]	416.20[c]
B (10^6 G)	15 [a]	800 [c]
B_{quad} (G)	Unconstrained	Unconstrained
M_d ($M_\odot$)	0.30	0.34
$\dot{M}$ ($10^{-7}\,M_\odot$ s^{-1})	2.62	8.0
M_{loss} ($M_\odot$)	0.20	0.17
Δt_{obs} (Gyr)	2.66	0.096

Notes. There are two possible solutions for the mass of the DWD components, M_1 and M_2, corresponding to the two values of the binary mass ratio, q_a and q_b, that solve the system constraints (see Figures 7 and 8). Δt_{obs} is the rotational age, i.e., the total time elapsed since the merger to the instant when the WD reaches the current measured rotation period. We recall that we constrain the system to have Δt_{obs} equal to the estimated WD cooling age. See the text for further details.

References.
[a] Kilic et al. (2021b).
[b] Kilic et al. (2021a).
[c] Caiazzo et al. (2021).

measured mass, magnetic field strength, and cooling age to infer the mass accretion rate and the disk mass.

The results of this article are the first attempt to establish a direct link between observed HFMWDs and their DWD merger progenitors. We conclude that the observed parameters of J2211+1136 and J1901+1458 are consistent with a DWD merger origin, and we have obtained the mass of the premerger

DWD primary and secondary binary components (see Table 1). Interestingly, the derived parameters of the merging DWDs are in line with those of known DWDs (like NLTT 12758; see Kawka et al. 2017), which further supports the connection between HFMWDs and DWD mergers.

If HFMWDs like J2211+1136 and J1901+1458 are DWD merger products, the newborn merged remnant, besides being massive and highly magnetic, might be fast rotating in its early postmerger life (e.g., in its first 1–100 kyr; see Figures 4 and 6). WDs with such extreme properties might power a variety of transient and persistent electromagnetic phenomena in astrophysical sources. For instance, Schwab (2021a) discusses evolutionary models of DWD merger remnants and how they might experience a $\sim$10 kyr luminous giant phase during their final approach to the single massive WD or a NS fate.

The DWD merger and its early activity can also lead to low-energy gamma-ray bursts. Phenomena in the merged magnetosphere can power the prompt gamma-ray emission, the cooling of the expanding ($\sim 10^{-3} M_\odot$) ejecta can power an infrared/optical transient days to week postmerger, and synchrotron emission of the ejecta and the WD pulsar-like emission can lead to extended (years) X-ray, optical, and radio emission (Rueda et al. 2019, 2022).

Massive, fast-rotating HFMWDs with pulsar-like activity might show up as magnetars (see, e.g., Malheiro et al. 2012; Rueda et al. 2013; Coelho & Malheiro 2014; Mukhopadhyay & Rao 2016; Coelho et al. 2017; Cáceres et al. 2017; Becerra et al. 2018; Borges et al. 2020, and references therein). Other high-energy phenomena involving DWD mergers and HFMWD products are the emission of high-energy neutrinos (see, e.g., Xiao et al. 2016) and particle acceleration leading to very-high-energy ($\gtrsim 10^{15}$ eV) and ultra-high-energy ($\gtrsim 10^{18}$ eV) cosmic rays. In addition, space-based detectors of gravitational waves (GWs) like the Laser Interferometer Space Antenna expect to detect the GW radiation driving the dynamics of compact, detached DWDs (see, e.g., Stroeer & Vecchio 2006; Korol et al. 2022). Electromagnetic radiation phenomena might affect the evolution of merging DWDs detectable through the deviations from the case when pure GW radiation drives the orbital dynamics (see Carvalho et al. 2022, and references therein), and the fast rotation and high magnetic fields might also lead to GW radiation from HFMWD pulsars (see, e.g., Sousa et al. 2020a, 2020b).

ORCID iDs

M. F. Sousa ⬤ https://orcid.org/0000-0002-5438-3460
J. G. Coelho ⬤ https://orcid.org/0000-0001-9386-1042
J. C. N. de Araujo ⬤ https://orcid.org/0000-0003-4418-4289
S. O. Kepler ⬤ https://orcid.org/0000-0002-7470-5703

J. A. Rueda ⬤ https://orcid.org/0000-0003-4904-0014

References

Bagnulo, S., & Landstreet, J. D. 2022, ApJL, 935, L12
Becerra, L., Boshkayev, K., Rueda, J. A., & Ruffini, R. 2019, MNRAS, 487, 812
Becerra, L., Rueda, J. A., Lorén-Aguilar, P., & García-Berro, E. 2018, ApJ, 857, 134
Benz, W., Cameron, A. G. W., Press, W. H., & Bowers, R. L. 1990, ApJ, 348, 647
Blouin, S., & Daligault, J. 2021, ApJ, 919, 87
Borges, S. V., Rodrigues, C. V., Coelho, J. G., Malheiro, M., & Castro, M. 2020, ApJ, 895, 26
Cáceres, D. L., de Carvalho, S. M., Coelho, J. G., de Lima, R. C. R., & Rueda, J. A. 2017, MNRAS, 465, 4434
Caiazzo, I., Burdge, K. B., Fuller, J., et al. 2021, Natur, 595, 39
Carvalho, G. A., dos Anjos, R. C., Coelho, J. G., et al. 2022, ApJ , 940, 90
Cheng, S. 2020, in IAU Symp. 357, White Dwarfs as Probes of Fundamental Physics: Tracers of Planetary, Stellar and Galactic Evolution, ed. M. A. Barstow et al. (Cambridge: Cambridge Univ. Press), 175
Cheng, S., Cummings, J. D., Menard, B., & Toonen, S. 2020, ApJ, 891, 160
Coelho, J. G., Cáceres, D. L., de Lima, R. C. R., et al. 2017, A&A, 599, A87
Coelho, J. G., & Malheiro, M. 2014, PASJ, 66, 14
Dan, M., Rosswog, S., Bruggen, M., & Podsiadlowski, P. 2014, MNRAS, 438, 14
Ferrario, L., de Martino, D., & Gänsicke, B. T. 2015, SSRv, 191, 111
García-Berro, E., Lorén-Aguilar, P., Aznar-Siguán, G., et al. 2012, ApJ, 749, 25
Guerrero, J., García-Berro, E., & Isern, J. 2004, A&A, 413, 257
Illarionov, A. F., & Sunyaev, R. A. 1975, A&A, 39, 185
Kalogera, V., Narayan, R., Spergel, D. N., & Taylor, J. H. 2001, ApJ, 556, 340
Kawka, A., Briggs, G. P., Vennes, S., et al. 2017, MNRAS, 466, 1127
Kepler, S. O., Pelisoli, I., Koester, D., et al. 2016, MNRAS, 455, 3413
Kepler, S. O., Winget, D. E., Vanderbosch, Z. P., et al. 2021, ApJ, 906, 7
Kilic, M., Bergeron, P., Blouin, S., & Bédard, A. 2021a, MNRAS, 503, 5397
Kilic, M., Kosakowski, A., Moss, A. G., Bergeron, P., & Conly, A. A. 2021b, ApJL, 923, L6
Korol, V., Hallakoun, N., Toonen, S., & Karnesis, N. 2022, MNRAS, 511, 5936
Külebi, B., Jordan, S., Euchner, F., Gansicke, B. T., & Hirsch, H. 2009, A&A, 506, 1341
Longland, R., Lorén-Aguilar, P., José, J., García-Berro, E., & Althaus, L. G. 2012, A&A, 542, A117
Lorén-Aguilar, P., Isern, J., & García-Berro, E. 2009, A&A, 500, 1193
Malheiro, M., Rueda, J. A., & Ruffini, R. 2012, PASJ, 64, 56
Maoz, D., & Hallakoun, N. 2017, MNRAS, 467, 1414
Maoz, D., Hallakoun, N., & Badenes, C. 2018, MNRAS, 476, 2584
Menou, K., Esin, A. A., Narayan, R., et al. 1999, ApJ, 520, 276
Mukhopadhyay, B., & Rao, A. R. 2016, JCAP, 2016, 007
Pétri, J. 2015, MNRAS, 450, 714
Pringle, J. E., & Rees, M. J. 1972, A&A, 21, 1
Raskin, C., Scannapieco, E., Fryer, C., Rockefeller, G., & Timmes, F. X. 2012, ApJ, 746, 62
Rueda, J. A., Boshkayev, K., Izzo, L., et al. 2013, ApJL, 772, L24
Rueda, J. A., Ruffini, R., Li, L., et al. 2022, IJMPD, 31, 2230013
Rueda, J. A., Ruffini, R., Wang, Y., et al. 2019, JCAP, 2019, 044
Ruiter, A. J., Belczynski, K., & Fryer, C. 2009, ApJ, 699, 2026
Saio, H., & Nomoto, K. 1985, A&A, 150, L21
Schwab, J. 2021a, ApJ, 906, 53
Schwab, J. 2021b, ApJ, 916, 119
Schwab, J., Quataert, E., & Kasen, D. 2016, MNRAS, 463, 3461
Sousa, M. F., Coelho, J. G., & Araujo, J. C. N. 2020b, MNRAS, 498, 4426
Sousa, M. F., Coelho, J. G., & de Araujo, J. C. N. 2020a, MNRAS, 492, 5949
Stroeer, A., & Vecchio, A. 2006, CQGra, 23, S809
Wang, Y.-M. 1995, ApJL, 449, L153
Wickramasinghe, D. T., & Ferrario, L. 2000, PASP, 112, 873
Williams, K. A., Hermes, J. J., & Vanderbosch, Z. P. 2022, AJ, 164, 131
Xiao, D., Mészáros, P., Murase, K., & Dai, Z. -G. 2016, ApJ, 832, 20
Zhu, C., Chang, P., van Kerkwijk, M. H., & Wadsley, J. 2013, ApJ, 767, 164